Photovoltaics

Aldo Di Carlo(*), Enrico Lamanna(**) and Narges Yaghoobi Nia(***)
CHOSE – University of Rome Tor Vergata - Roma, Italy

Summary. — The conversion of solar energy into electricity via the photovoltaic (PV) effect has been rapidly developing in the last decades due to its potential for transition from fossil fuels to renewable energy based economies. In particular, the advances in PV technology and on the economy of scale permitted to reduce the cost of the energy produced with solar cells down to the energy cost of conventional fossil fuel. Thus, PV will play an important role to address the biggest challenges of our planet including global warming, climate change and air pollution. In this paper, we will introduce the photovoltaic technology recalling the working principle of the photovoltaic conversion and describing the different PV available on the market and under development. In the last section, we will focus more on the emerging technology of the halide perovskite, which is the research subject of the authors.

1. – Introduction

The amount of power impinging the Earth's surface in a year from the Sun is on average roughly 1.5×10^9 TWh, while from fig. 1(a) we observe that the World's yearly energy consumption is less than 14000 Mtoe, amounting to 1.6×10^5 TWh. Thus, the

(*) E-mail: aldo.dicarlo@uniroma2.it
(**) E-mail: enrico.lamanna@uniroma2.it
(***) E-mail: narges.yaghoobi.nia@uniroma2.it

amount of energy we receive from the Sun in a year on Earth is 10000 times the world energy requirements. From this, we understand that even with photovoltaic (PV) systems with a seemingly low (and already commercially available) Power Conversion Efficiency of 20% uniformly covering 0.1% of the Earth surface (roughly the dimension of Spain) we could satisfy the World's energy demand for the year. Of course, this computation is speculative and merely serves as an example, but it gives an idea of the potential of solar energy conversion on the request of renewable energy. At the same time, other renewable energy sources, such as hydroelectric, wind, and geothermal, can and will contribute to the renewable energy production, especially considering the fact that day-night cycles and the cloudy days make solar energy an intermittent or variable source.

One of the factors that limited the pervasive use of photovoltaics was the high cost, with respect to fossil fuels of the generated electricity. In fact, the cost of power generation is a general limiting factor for renewable energy technologies: a very efficient electricity generation system may be very expensive, hence not so convenient. However, due to the increased production capacity and the improved performances the cost of PV energy has been highly reduced in the last years; from 2010 to 2019 it has been reduced by a factor ~ 5 as shown in fig. 1(b), (c). Nowadays the cost of PV installation can be lower than 1000 \$/kW (fig. 1(b)) with a cost of PV modules down to 0.3 \$/Wp. The levelized cost of electricity (LCOE) is a useful metric to compare different energy sources and it is defined as the total cost of an energy system divided by the duration of its useful lifetime [1]. At the time of writing, the global average of LCOE for PVs is 68 \$/MWh (fig. 1(c)) and ranges between 50 and 180 \$/MWh, depending on the solar panel technology and on the size of the installation, with values as low as of 20–25 \$/MWh in sun-rich areas. This makes photovoltaics very competitive with fossil fuels, which currently range between 43 and 150 €/MWh([1]). All this considered, it is trivial to see that photovoltaics will play a key role in this evolutionary strive towards ethical and sustainable survival of the human race on Earth.

In this short introduction to the photovoltaic technologies, we will recall the working principle of the photovoltaic conversion and then we will describe the different approaches to solar cell developments. In the last section, we will focus more on the emerging technology of the halide perovskite, which is the research subject of the authors.

2. – Solar cell working principle

The working principle of a solar cell can be made easy considering that we need two main mechanisms to convert sun light into electricity: i) the light should be absorbed and electrons and holes should be generate in the conduction and valence band, respectively; ii) the generated electrons and holes should be separated and transported to their selective contact. This is summarized in fig. 2.

As we can see from the figure, the light, with photon energy bigger that the Light

([1]) IRENA, International Renewable Energy Agency.

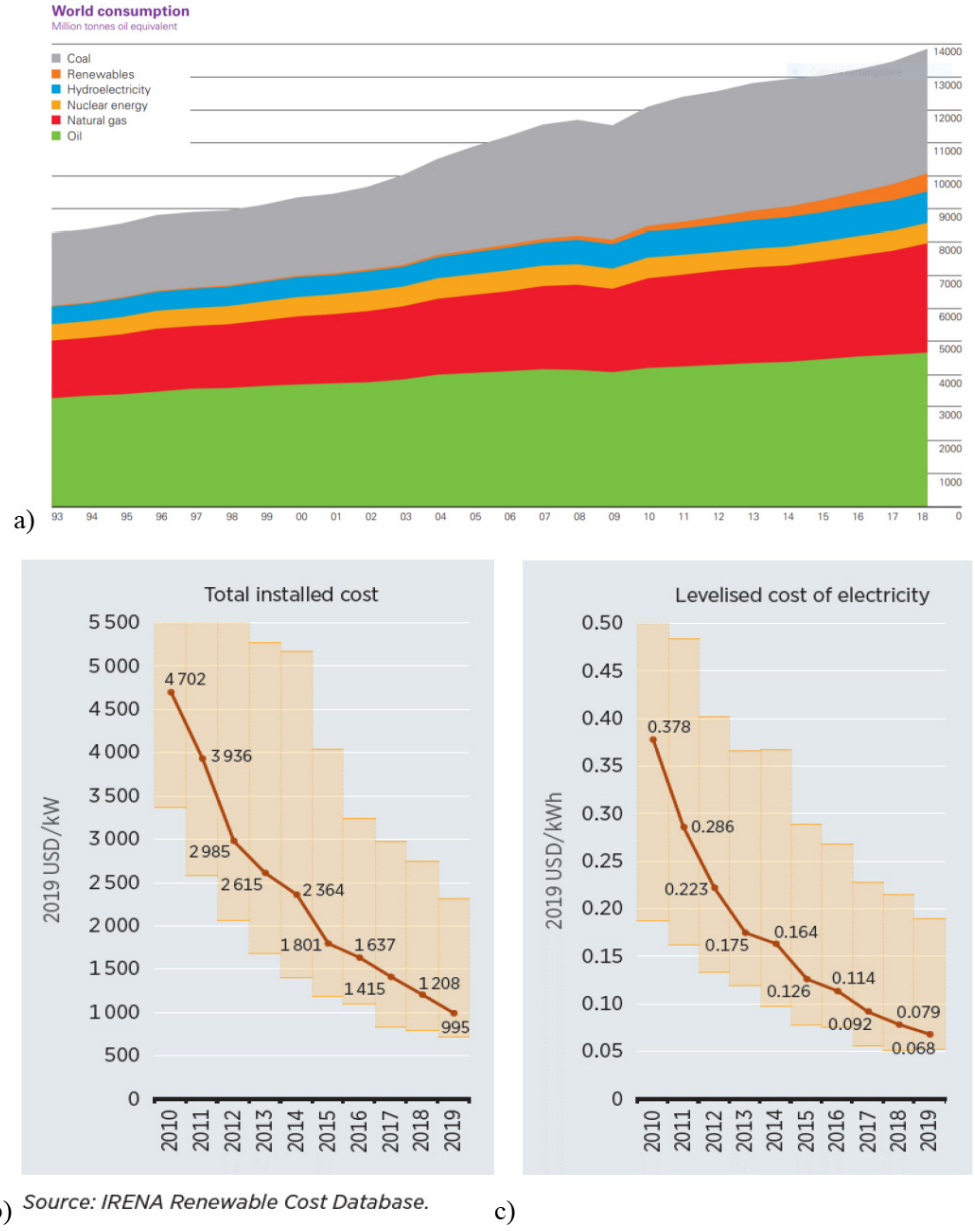

Fig. 1. – Statistical review: (a) the graph shows the global trend of energy sources consumption starting 1993 up to 2018. Taking into account coal (in grey), renewable sources (solar, wind and geothermal in orange), hydroelectric (in blue), nuclear (in light orange), natural gas (in red) and oil (in green) [2]. Global weighted average (b) total installed costs and (c) LCOE for PV, 2010–2019. The bars represent the interval between the 95th and 5th percentile. (Adapted from `https://www.irena.org/publications/2020/Jun/Renewable-Power-Costs-in-2019`.)

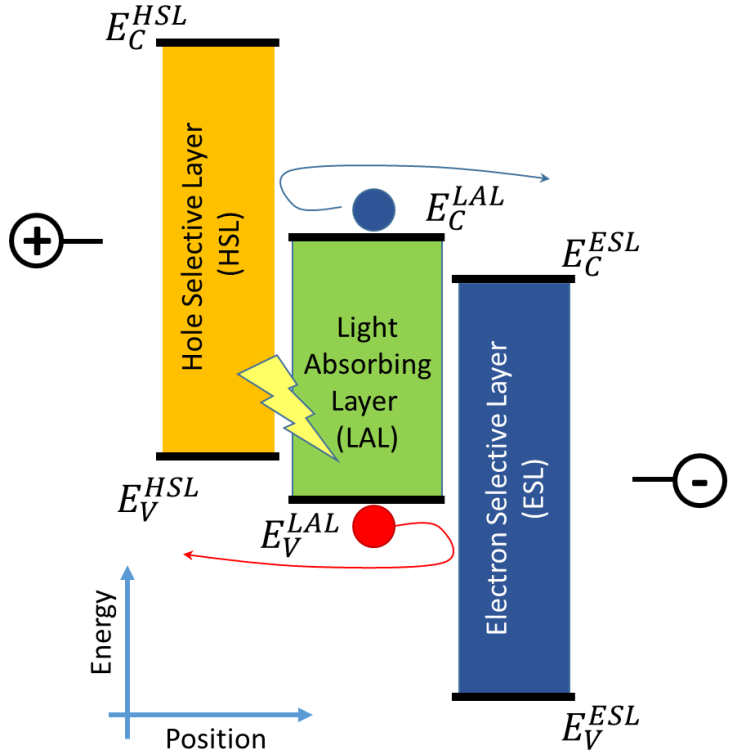

Fig. 2. – Schematic diagram of key elements for solar cells. Three, eventually different, materials are used for the Hole Selective Layer (HSL) the Electron Selective Layer (ELS) and the Light Absorbing Layer (LAL). The coloured areas depict the bandgap of the materials while $E_C^{:L}$ and $E_V^{:L}$ the conduction and valence edges of the layer L, respectively.

Absorbing Layer (LAL) energy gap, is absorbed in LAL and the generated electrons and holes will diffuse in the layer. If an electron reaches the interface between the LAL and the Electron Selective Layer (ESL), due to the favourable band alignment, it is transferred into the ESL and can reach the electrode. On the opposite, if an electron reaches the interface between the LAL and the Hole Selective Layer (HSL), the presence of the HSL gap prevent the charge transfer and the electron is reflected back. This device asymmetry permits the electrons to move toward the negative electrode of the cell (apart possible recombination with holes). Similarly, holes are easily transfered from LAL to HSL while they are reflected when they reach the LAL/ESL interface. Consequently, holes move toward the positive electrode. We should point out that the device asymmetry is related to the particular "staggered" alignment of the conduction and valence band edges of the layers.

The conceptual scheme presented in fig. 2 can be practically implemented by using homojunctions (same material for all the three layers) of by using heterojunctions where different materials are used for the layers. For the homojunction solar cell, the staggered alignment of the band edges is obtained by specific doping of the layers exploiting the concept of the p-n junction. On the other hand, heterojuction solar cells rely mainly on

the different position of the conduction and valence band of the HSL, LAL and ESL.

2˙1. *Homojunction solar cells.* – The simplest homojunction solar cell can be realized by using a single p-n junction, meaning the junction between a *p-type* semiconductor and an *n-type* semiconductor. This feature of semiconductors can be controlled by *doping*, which in its simplest form consists in substituting atoms in the lattice of the material with other elements having higher valency (donors) or lower valency (acceptors). These donor and acceptor states are close to the band edges and can easily transfer the charge, via thermal excitation into the conduction (electron from donor states) or valence (hole from acceptor state) bands. As an example, silicon is a semiconductor material with a bandgap of 1.12 eV. It is a group-IV element, therefore is has valency 4, and the doping is often performed by substitution of some atoms with boron (III) atoms for p-doping, or phosphorus (V) atoms for n-doping. Because of the doping free charge carriers are introduced in the bands of the semiconductors, n-type semiconductors have a higher electron density in the conduction band, and similarly p-type semiconductors will have a higher density of holes in the valence band. Upon forming the p-n junction, the higher concentration of electrons in the n-type, compared to the p-type semiconductor, will induce a diffusion of negative carriers from the n-type semiconductor to the p-type; conversely, holes will diffuse from the p-type to the n-type. This flow of charge will continue until thermal equilibrium is reached and it induces the formation of a space charge region (or depletion region) with no free charge carriers present in it. A positive charge builds up at the n-side of the interface between the two semiconductors, while an equal negative charge gathers to the p-side, resulting in an electric field being present across the whole depletion region opposing further diffusion of charges. As a matter of fact, the presence of the electric field will drift all excess electrons going through the space charge region towards the n-side, while holes will drift to the p-side of the junction. Equilibrium is reached when the drift and diffusion current for both electrons and holes match each other. Looking at the band diagram of fig. 3(a) the formation of a depletion zone with net charge density (ρ) of opposite sign will create an electric field that, in turn, will bend the band profile across the depletion region. The potential difference between the two extremes of the space charge region is called built-in potential and is related to the difference between the Fermi levels of the two sides of the junction: a stronger doping of both sides will induce a higher built-in potential and a smaller depletion region.

As we can notice from fig. 3(b) the p-n junction resembles the junction between the LAL and the ESL: electron photoexcited in the LAL could move in the ESL, while photoexcited holes are reflected back at this interface. Clearly, in this simplified solar cell only one charge selective layer is used, nevertheless it create the required asymmetry for cell functioning.

Let us now consider more in detail the absorption and transport process. If a photon has an energy higher or equal to the energy gap of the semiconductor, then it can be absorbed forming an exciton (*i.e.*, an electron-hole pair in an excited state). If the binding energy between the carriers is higher than thermal energy, the charge are strongly bonded and will recombine, otherwise the photon absorption will result in the formation

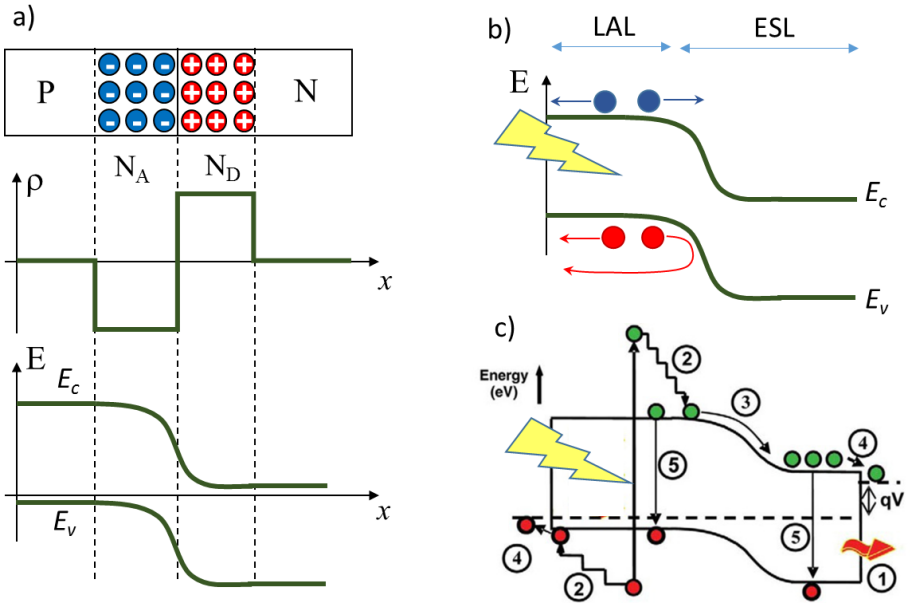

Fig. 3. – (a) p-n junction and band alignment. Schematics of a p-n junction representing the distribution of charge after the thermal equilibrium and the formation of the depletion or space charge region ρ. Notice how the area of the two rectangles is the same, meaning the accumulated charge is the same in order to have neutrality of charge within the junction. The conduction and valence band profiles of the p-n junction obtained by aligning the Fermi levels of both sides. (b) Absorbing and selective layers: photon absorbed in the P region can generate electron and holes, but due to the presence of the junction barrier, only electrons can move in the N region. By using the p-n junction we have implemented the LALA/ESL interface. (c) Charge transport and recombination processes after photon absorption. All the different processes which could be involved after illuminating a p-n junction: 1) non-absorption of low energy photons; 2) thermalization of high energy carriers (or Auger recombination); 3) charge drifted to the collection electrode; 4) charge collected at the electrode; 5) non-radiative recombination.

of a free electron in the conduction band and a free hole in the valence band. These photo-generated carriers will have an average energy described by the quasi-Fermi levels for electrons and holes. The difference between the quasi-Fermi levels (called quasi-Fermi levels splitting and abbreviated QFLS) is the upper limit to the potential that can be extracted from the illuminated semiconductor. If the energy of the photon is lower than the energy gap, then the material will be transparent to that radiation. All photons with energy higher than the bandgap will actually excite electrons to higher energy levels than the conduction band minimum (or holes lower than the valence band maximum). However, this "extra" energy will be lost through a process called thermalization, in which eventually it released to the lattice of the material, resulting in an increase in temperature of the junction. After photo-generation, charge carriers have to travel to the contacts where they are selectively collected. In the process, charges may incur in different phenomena all schematized and marked by a number in fig. 3(c):

– They diffuse (or are drifted (3), depending on the technology) towards the respective selective contact (4);

– The electron-hole pair recombines and transfers the energy to another electron or hole, which move further up in the conduction band or down in the valence band, respectively. These charges then thermalize and energy is lost (Auger Recombination (2));

– The electron-hole pair recombines (5) and the energy is lost as heat (non-radiative recombination). This process is often assisted by trap states in the bandgap, which come from defects in the material (Shockley-Reed-Hall, SRH recombination);

– The electron-hole pair recombines and a photon is reemitted in turn (radiative recombination), and it may be reabsorbed and photo-generate a new electron-hole pair.

This last process is very favourable and is common in direct bandgap materials with a high degree of purity and a low density of defects. It is commonly referred to as *photon recycling* and accounts for part of the charge transport in some materials, rather than diffusion or drift processes [3].

The defects in the material contributing to the formation of mid-gap trap states and to SRH recombination phenomena may come from bulk impurities, lattice vacancies (sometimes caused by doping), dangling bonds and surface defects. In a conventional crystalline silicon p-n junction the probability of an electron-hole pair to recombine is higher the further it is from the depletion region where the electric field would separate the two carriers and send them to the respective selective electrodes. The average distance that a carrier can travel before recombining is called diffusion length (L) and has a strong dependence on the quality of the material, hence the carrier lifetime (τ) and the mobility of the carriers (μ):

$$L = \sqrt{\frac{kT\tau\mu}{q}}\,.$$

The carrier lifetime depends on the probability of each non-radiative recombination process (SRH or Auger).

So, when the p-n junction is in dark, its current (J_{dark}) is determined by the Shockley ideal diode equation

$$J_{dark} = J_0 \left(e^{\frac{qV}{nkT}} - 1\right),$$

in which V is the applied voltage, n is an ideality factor, generally equal to 1 for indirect gap semiconductors and 2 for direct gap semiconductors (but can be any value between these, according to the rate of non-radiative recombination), and J_0 is the dark saturation current (mostly depending on doping and diffusion length). As light is shone on the junction, minority carriers concentration increases on both sides and they will diffuse

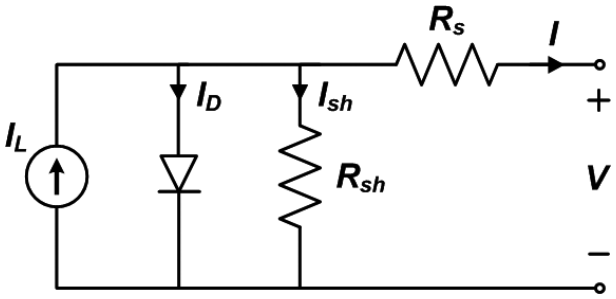

Fig. 4. – Equivalent circuit of a solar cell. Simplistic circuit modelling of a solar cell, with a current generator and a diode in parallel to it to show the diode-like behaviour. Series and shunt resistances are added in series and parallel, respectively, to account for non-idealities in real device behaviour and changes to the current-voltage characteristics.

towards the space charge region. This means that an electron current will flow from the p-side to the n-side, while the hole current will flow from the n-side to the p-side: following the general convention on charge flow and electric current direction, a net electric current flows from the n- to the p-side, and therefore, opposite to the diode current J_{dark}. The total current is

$$J = J_{dark} - J_{light}.$$

The J_{light} is commonly referred to as short-circuit current (J_{sc}) and it is the maximum current which can be collected from the device. The name short circuit comes from its definition: it is the current flowing through the illuminated junction when its electrodes are short-circuited.

From an electrical point of view, we could simplistically model a solar cell as the electric circuit represented in fig. 4.

The Shockley ideal diode equation does not take into account resistive losses of real-world devices, therefore it can be adjusted by looking at the equivalent circuit and considering that the output voltage to the cell will undergo a drop related to the series resistance:

$$V_{Rs} = J \cdot R_s$$

and for the output current the shunt losses due to the bound value of R_{sh} will result in

$$J = J_0 \left(e^{\frac{qV}{nkT}} - 1 \right) - J_{SC} + \frac{V + J \cdot R_s}{R_{sh}} .$$

Therefore, as R_s increases the curve deviates from the ideal diode behaviour and the same happens for low values of R_{sh}. The trend is shown in fig. 5.

From the representative JV curves of fig. 5 it is evident that, within a reasonable range of values, the intersections of the characteristics with the axes do not depend on

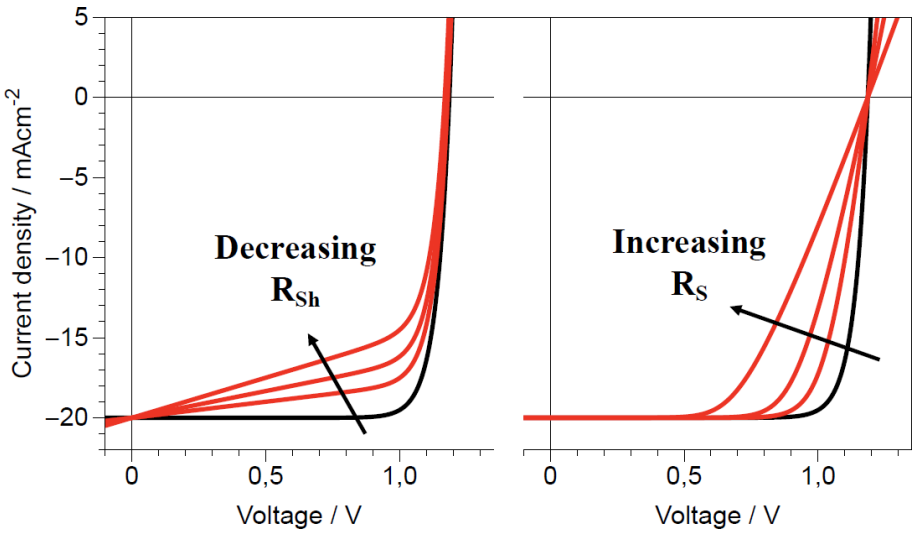

Fig. 5. – Effect of non-idealities on the current-voltage characteristics of a solar cell. On the left the effect of decreasing shunt resistance, which should ideally be equal to infinity; on the right the effect of increasing series resistance, which should ideally be equal to zero.

these non-ideal electrical behaviours. The point where the curve meets the y-axis is the short-circuit current, that we have already defined; the intersection with the x-axis is the open circuit voltage (V_{OC}), defined as the output voltage measured when no current flows through the cell, so with floating contacts (open circuit) and can be derived by the

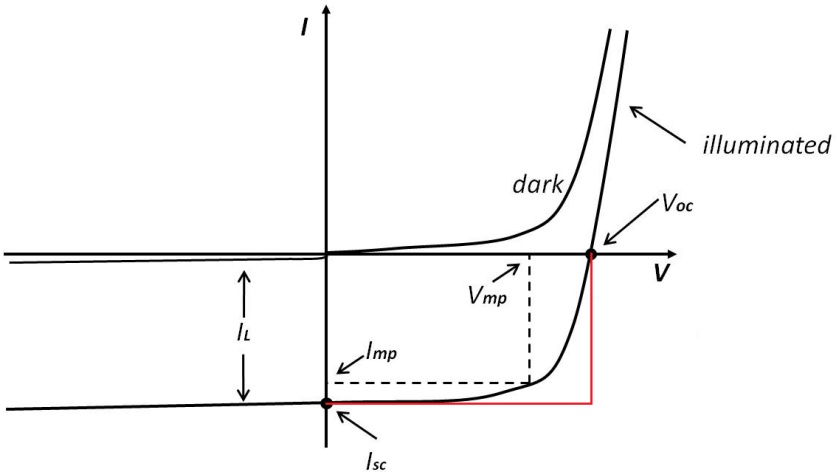

Fig. 6. – Example current-voltage curve of a real solar cell. A solar cell JV curve and its FoM.

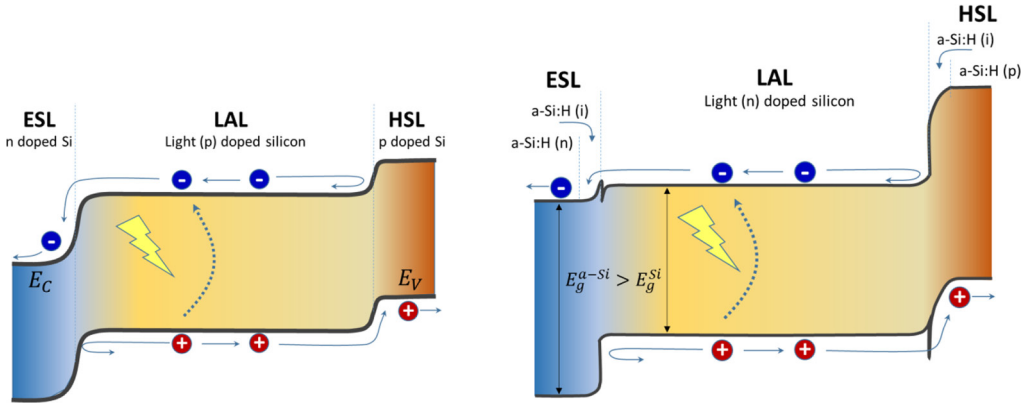

Fig. 7. – (a) Band profile of Passivated Emitter Rear Cell (PERC) based on homojunction silicon technology; (b) band profile of a heterojunction a-Si/c-Si solar cell.

following equation:

$$V_{OC} = \frac{nkT}{q} \cdot \ln\left(\frac{J_{SC}}{J_0} + 1\right).$$

Finally, after briefly analysing the physics and electronics behind the functioning mechanisms of solar cells [4,5], we may now define their figures of merit (FoM). The short-circuit current and the open circuit voltage have already been defined. These two values depend only on the quality of the materials composing the device. Another fundamental parameter is the Fill Factor, which summarizes the effect of series and shunt resistance on the performance of the device and gives an idea of the deviation of the real solar cell from the ideal diode behaviour, as can be seen from fig. 6:

$$FF = \frac{V_{MP} \cdot I_{MP}}{V_{oc} \cdot I_{sc}}.$$

Last, but not least, the power conversion efficiency (PCE) of the solar cell, which depends on all the other FoM and is simply defined as the ratio

$$PCE = \eta = \frac{\text{Generated Power}}{\text{Incident Power}} = \frac{P_{out,\,max}}{P_{inc}} = \frac{V_{MP} \cdot I_{MP}}{P_{inc}} = \frac{V_{oc} \cdot I_{sc} \cdot FF}{P_{inc}}.$$

The maximum power point ($P_{out,\,max}$) and its current (I_{MP}) and voltage (V_{MP}), must be imposed by adapting the load of the solar device and have to be followed by a maximum power point tracker (MPPT) to adjust to any environmental or electrical modifications.

Even if the concept of p-n solar cell has been very beneficial for the development of the field, the modern implementations of homojunction solar cell (like silicon solar cells) consider the general structure of fig. 2 where all the selective layers are considered. To

add an additional selective layer to the p-n junction scheme developed above we can make use of something similar to the p-n junction as shown in fig. 7(a).

Here the LAL, represented by lightly doped (or almost intrinsic) silicon has an ELS realized with a p-n junction, while the HLS is obtained by a p^-p^+ junction (where p^+ means a heavily doped p layer). This scheme is at the base of the Passivated Emitter Rear Cell (PERC) which is now more and more entering into the production market.

2˙2. *Heterojunction solar cells.* – In the heterojunction solar cells, some or all the layers forming the cell can be made by a different material. A very popular family of heterojunction cells is the amorphous/crystalline silicon heterojunction, better known as silicon heterojunction and abbreviated SHJ (which Panasonic trademarked HIT). These devices, together with their homo-junction counterpart PERL cells probably offer the best performance for silicon-based PV. However, compared to these, silicon heterojunctions require lower processing temperatures and no photolithographic processes, resulting in cheaper fabrication. The idea behind the SHJ cell is that the junction may be formed between crystalline silicon (c-Si) and hydrogenated amorphous silicon (a-Si:H) layers deposited by Plasma Enhanced Chemical Vapour Deposition (PECVD), which also serve as passivating layers, hence the name heterojunction. The oppositely doped a-Si:H layers at the sides of the cell are charge selective contacts, as they energetically favour the transport of a specific type of charge carriers and block the opposite charges. A general structure and energy band profile are shown in fig. 7(b). As shown in the figure, by properly doping the a-Si it is possible to create the staggered structure where holes (electrons) are reflected back by the ESL (HSL).

The good passivation coming from the use of a-Si:H yields higher open circuit voltages. Furthermore, the possibility to avoid high-temperature doping-by-diffusion processes allows using thinner wafers thus further reducing recombinations and further improving the open circuit voltage, as previously mentioned. On the other hand, the low lateral conductivity of amorphous silicon forces the use of transparent conductive oxides (TCO) as electrodes, especially on the front surface, where lateral conductivity is key to have efficient extraction at the metal grid fingers [6]. Since the most used TCO is Indium Tin Oxide (ITO), the high cost of this material, related to the scarcity of indium, is a reason of concern. Because of the dehydrogenation of the amorphous silicon, all the fabrication steps must be carried out at $T < 200\,^\circ\mathrm{C}$, which adds complexity and limits the possible materials and processes to use in combination with this technology. Another drawback related to silicon heterojunctions is the unfavourable band alignment of p-type c-Si wafers with doped amorphous silicon, which limits the application of p-type wafers that are the cheapest and most widely used in electronics. Lastly, the 1.7 eV gap of amorphous silicon causes it to have a parasitic absorption in the visible spectrum, meaning that it should be as thin as possible. In fact, because of the high binding energy and low diffusion length of amorphous silicon, charges photo-excited inside the amorphous layers will recombine quickly [7]. Other materials may be used to substitute a-Si:H, like amorphous or nanocrystalline silicon oxide [8]. The 26.7% efficiency record for crystalline silicon solar cells was obtained with a silicon heterojunction solar cell with interdigitated

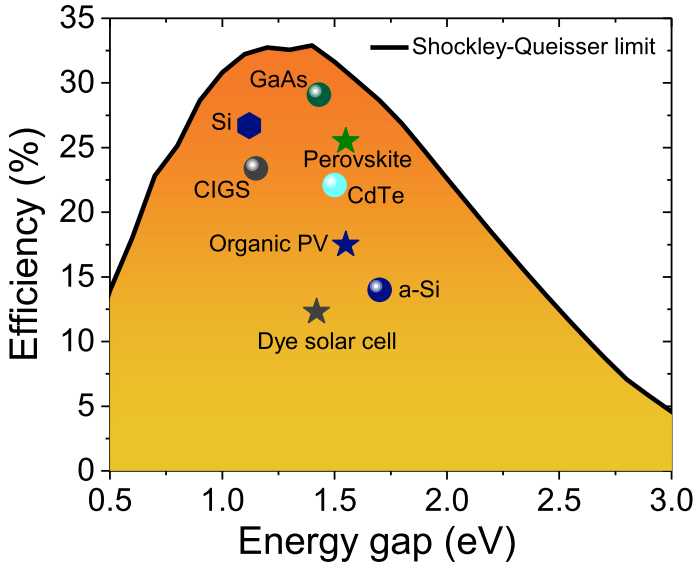

Fig. 8. – Theoretical Shockley-Queisser efficiency limit as a function of the bandgap (black line) [12]. The record efficiencies for different absorber materials are plotted for the corresponding bandgaps. Hexagons symbols are related to crystalline materials, circles to thin-film PV while stars to emerging PV.

back contacts (IBC), which means that the architecture of the cell has been optimized so that both electrodes are at the back of the cell and do not cause any shadowing on the device [9]. Other heterojunction solar cells will be discusses in the next section.

To conclude this section, just a remark on the maximum attainable PCE. The first evaluation of the efficiency limit of an illuminated p-n junction was performed by Shockley and Queisser in 1961 [10]. In their detailed balance analysis, they estimated that the efficiency of a 1.1 eV bandgap semiconductor could achieve a maximum efficiency of 30%. Subsequent studies have updated the limit for the ideal p-n junction with a 1.3 eV bandgap to 33.7% [11]. This is known as the Shockley-Queisser (SQ) limit for an ideal single-junction solar cell. Figure 8 shows the SQ limit as a function of the bandgap of the absorbing material. The efficiency obtained for different PV technologies (see next section) are also displayed.

The SQ calculation, however, starts from some assumptions of ideality, which are basically non-existent in real devices:

- The absence of resistive losses;
- Only radiative recombinations occur, all the other loss mechanisms (SRH and Auger) are not accounted for;
- No thermalization losses;

– A single photon contributes to the excitation of a single electron;

– No possibility to concentrate light.

A more recent study has set the limit efficiency for crystalline silicon to 29.7% under non-concentrated sunlight [13]. All these estimates are valid for single-junction non-concentrator solar cells, but are not true for multijunction solar cells and/or devices working with concentrated light([2]). This is where tandem solar cells come into play, allowing to overcome these limits and, therefore, enabling lower LCOE costs for PV systems [14].

3. – Photovoltaic technologies

Following from the previous section, since 1954 and the first crystalline silicon p-n junction a lot of progress has been made in the field of photovoltaics. So much that now the materials involved in the making of photovoltaic devices are not just limited to silicon, nor to inorganic semiconductors. As a matter of fact, various generations of photovoltaics have made their appearance, each of them having pros and cons.

Solar cell technologies are typically named according to their primary light-absorbing material. As shown in fig. 9, we can classify PV technologies using two categories: wafer-based and thin-film cells. Wafer-based cells are fabricated on semiconducting wafers and can be handled without an additional substrate, although modules are typically covered with glass for mechanical stability and protection. Thin-film cells consist of semiconducting films deposited onto a glass, plastic, or metal substrate. Moreover, we can further classify thin films into commercial and emerging thin-film technologies.

3˙1. *Wafer-based PV*. – Three primary wafer-based technologies exist today:

– *Crystalline silicon (c-Si)* solar cells constitute $\sim 90\%$ of current global production capacity and are the most mature of all PV technologies. Silicon solar cells are classified as single-crystalline (sc-Si) or multicrystalline (mc-Si), with respective market shares of $\sim 35\%$ and $\sim 55\%$ in 2014 [16]. Cylindrical single crystals are typically grown by Czochralski (CZ) [17] or float-zone (FZ) methods, while mc-Si blocks are formed by casting. The resulting ingots are sliced into 150–180 μm wafers prior to cell processing. As discussed before, the high-efficiency sc-Si variant is the heterojunction SHJ. Multicrystalline cells contain randomly oriented grains with sizes of around 1 cm^2. Grain boundaries hinder charge extraction and reduce mc-Si performance relative to sc-Si. Record cell efficiencies stand at 26.7% for sc-Si and 23.3% for mc-Si [18]. One fundamental limitation of c-Si is its indirect bandgap, which leads to weak light absorption and requires wafers with thicknesses on the order of 100 μm in the absence of advanced light-trapping strategies. Key technological challenges for c-Si include stringent material

([2]) NREL, NREL Research Cell Record Efficiency Chart.

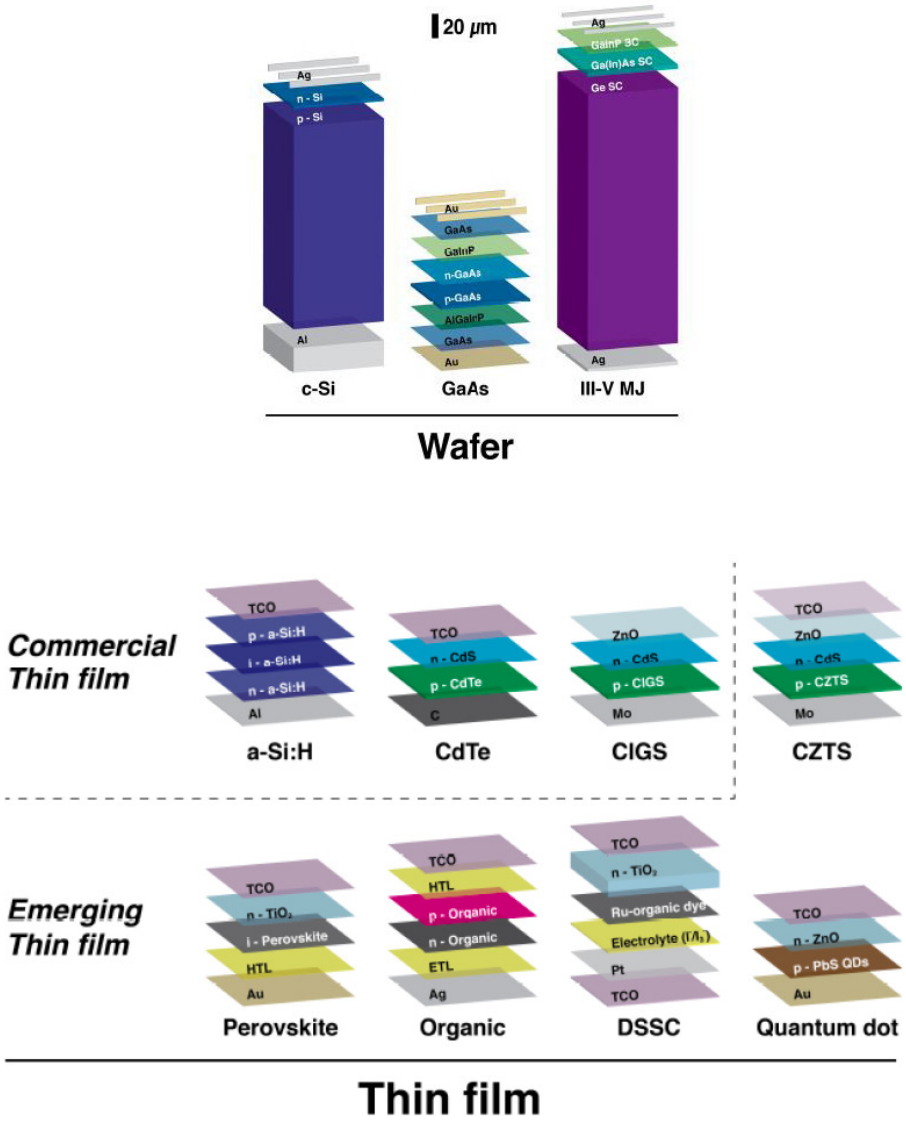

Fig. 9. – Typical solar PV device structures, divided into wafer-based and thin-film technologies. Primary absorber layers are labeled in white, and thicknesses are shown to scale. c-Si encompasses sc-Si and mc-Si technologies. GaAs cells use thin absorbing films but require wafers as templates for crystal growth. For III-V multijunctions, sub-cells are shown for the industry-standard GaInP/Ga(In)As/Ge triple-junction cell, and some interface layers are omitted for simplicity. A representative single-junction a-Si:H PV structure is shown here, although PV performance parameters used elsewhere correspond to an a-Si:H/nc-Si:H/nc-Si:H triple-junction cell. Front contact grids are omitted for thin-film technologies since the metals used for those grids do not directly contact the active layers and are thus more fungible than those used for wafer-based technologies. The figure is taken from ref. [15].

purity requirements, high material use, restricted module form factor, and batch-based cell fabrication and module integration processes with relatively low throughput.

– *Gallium arsenide (GaAs)* is almost perfectly suited for solar energy conversion, with strong absorption, a direct bandgap well matched to the solar spectrum (see fig. 8), and very low non-radiative energy loss. GaAs has achieved the highest power conversion efficiencies of any material system —29.3% for lab cells [18]. A technique known as epitaxial liftoff creates thin, flexible GaAs films and amortizes substrate costs by reusing GaAs wafers [19], but has not yet been demonstrated in high-volume manufacturing. Cost-effective production will require improved film quality, more substrate reuse cycles, and low-cost wafer polishing, which defines a cost floor for epitaxial substrates. High material costs may limit the large-scale deployment of GaAs technologies.

– *III-V multijunction (MJ)* solar cells use a stack of two or more single-junction cells with different bandgaps to absorb light efficiently across the solar spectrum by minimizing thermalization losses. Semiconducting compounds of group-III (Al, Ga, In) and group-V (N, P, As, Sb) elements can form high-quality crystalline films with variable bandgaps, yielding unparalleled power conversion efficiencies —46.0%, 44.4%, and 34.2% for record 4-junction (4J), 3J, and 2J cells, respectively, under concentrated illumination [18]. Record cell efficiencies without concentration are 38.8%, 37.9%, 31.6% for 4J, 3J, and 2J cells, respectively [18]. III-V MJs are the leading technology for space applications, with their high radiation resistance, low-temperature sensitivity, and high efficiency. But complex manufacturing processes and high material costs make III-V MJ cells prohibitively expensive for large-area 1-sun terrestrial applications. Concentrating sunlight reduces the required cell area by replacing cells with mirrors or lenses, but it is still unclear whether concentrating PV systems can compete with commercial single-junction technologies on cost. Current R&D efforts are focused on dilute nitrides (*e.g.*, GaInNAs) [20], lattice-mismatched (metamorphic) approaches [21], and wafer bonding [21, 22]. Key challenges for emerging III-V MJ technologies include improving long-term reliability and large-area uniformity, reducing materials use, and optimizing cell architectures for variable operating conditions. The vast majority of commercial PV module production has been —and is currently— c-Si, for reasons both technical and historical. Silicon can be manufactured into non-toxic, efficient, and extremely reliable solar cells, leveraging the cumulative learning of over 60 years of semiconductor processing for integrated circuits. Between sc-Si and mc-Si cells, the higher crystal quality in sc-Si cells improves charge extraction and power conversion efficiencies at the expense of more costly wafers (by 20% to 30%) and material processing. A key disadvantage of c-Si is its relatively poor ability to absorb light, which requires the use of thick, rigid, impurity-free, and expensive wafers. This shortcoming translates to high manufacturing capital costs and constrained module form factors. Despite these limitations, wafer-based c-Si will likely remain the leading deployed PV technology in the near future, and present c-Si technologies could conceivably achieve terawatt-scale deployment by 2050 without major technological advances. Current innovation opportunities include increasing mod-

ule efficiencies, reducing manufacturing complexity and costs, and reducing reliance on silver for contact metallization. Solar cells based on thin films of crystalline silicon can potentially bypass key limitations of conventional wafer-based c-Si PV while retaining silicon's many advantages and leveraging existing manufacturing infrastructure. Similarly to commercial thin-film technologies, thin-film c-Si PV can tolerate lower material quality (*i.e.*, smaller grains and higher impurity levels), uses 10–50× less material than wafer-based c-Si PV, may enable lightweight and flexible modules, and allows high-throughput processing. However, efficiencies for high-throughput-compatible approaches remain low compared to both wafer-based and leading commercial thin-film technologies, and manufacturing scalability is unproven. The only thin-film c-Si technology that has been commercialized to date was based on c-Si films on glass, but no companies remain in that market today.

3˙2. *Commercial thin-film PV*. – While c-Si currently dominates the global PV market, alternative technologies may be able to achieve lower costs in the long run. Solar cells based on thin semiconducting films now constitute $\sim$ 10% of global PV module production capacity [23]. Thin-film cells are made by additive fabrication processes, which may reduce material usage and manufacturing capital expense. This category extends from commercial technologies based on conventional inorganic semiconductors to emerging technologies based on nanostructured materials.

Key commercial thin-film PV technologies include the following:

– *Hydrogenated amorphous silicon (a-Si:H)* offers stronger absorption than c-Si, although its larger bandgap (1.7–1.8 eV, compared to 1.12 eV for c-Si) is not well matched to the solar spectrum. Amorphous silicon is typically deposited by plasma-enhanced chemical vapor deposition (PECVD) at relatively low substrate temperatures of 150–300 °C. A 300 nm film of a-Si:H can absorb $\sim$ 90% of above-bandgap photons in a single pass, enabling lightweight and flexible solar cells [24]. An a-Si:H cell can be combined with cells based on nano-crystalline silicon (nc-Si) or amorphous silicon-germanium (a-SiGe) alloys to form a multijunction cell without lattice-matching requirements. Most commercial a-Si:H modules today use multijunction cells. Silicon is cheap, abundant, and non-toxic, but while a-Si:H cells are well suited for small-scale and low-power applications, their susceptibility to light-induced degradation (the Staebler-Wronski effect [25]) and their low efficiency compared to other mature thin-film technologies (14% stabilized a-Si:H cell record [18]) limit market adoption.

– *Cadmium telluride (CdTe)* is the leading thin-film PV in the present global market. CdTe is a favorable semiconductor for solar energy harvesting, with strong absorption across the solar spectrum and a direct bandgap of 1.45 eV [24]. Record efficiencies of 22.1% for the cells and commercial module efficiencies continue to improve steadily [18]. CdTe technologies employ high-throughput deposition processes and offer the lowest module costs of any PV technology on the market today, although relatively high processing temperatures are required ($\sim$ 500 °C). Concerns about the toxicity of elemental cadmium [26] and the scarcity of tellurium have motivated research on alternative

material systems that exhibit similar simple manufacturing but rely on abundant and non-toxic elements.

– *Copper indium gallium diselenide ($CuIn_xGa_{1-x}Se_2$, or CIGS)* is a compound semiconductor with a direct bandgap of 1.1–1.2 eV. Like CdTe, CIGS films can be deposited by a variety of solution- and vapor-phase techniques on flexible metal or polyimide substrates [27], favorable for building-integrated and other unconventional PV applications. CIGS solar cells exhibit high radiation resistance, a necessary property for space applications. Record efficiencies stand at 23.4% for the concentrator cells [18]. Key technological challenges include high variability in film stoichiometry and properties, limited understanding of the role of grain boundaries [28], low open-circuit voltage due to structural and electronic inhomogeneity [29], and engineering of higher-bandgap alloys to enable multijunction devices [30]. Scarcity of indium could hinder large-scale deployment of CIGS technologies. The active materials used in commercial thin-film PV technologies absorb light 10–100 times more efficiently than silicon, allowing use of films just a few microns thick. Low materials use is thus a key advantage of these technologies. Advanced factories can produce thin-film modules in a highly streamlined and automated fashion. Furthermore, life cycle analyses suggest that thin films produce lower greenhouse gas emissions during production and use than c-Si PV (45 g CO_2-eq/kWh for c-Si [31], compared to 21, 14, and 27 g CO_2-eq/kWh for a-Si:H, CdTe, and CIGS, respectively [32]).

A key disadvantage of today's commercial thin-film modules is the comparatively low average efficiencies of 12–15%, compared to 15–21% for c-Si. Low efficiencies increase system costs due to area-dependent balance-of-system (BOS) costs such as wiring and mounting hardware. Most thin-film materials today are polycrystalline and contain much higher defect densities than c-Si. Some compound semiconductors such as CIGS have complex stoichiometry, making high yield, uniform, large-area deposition a formidable process-engineering challenge. Sensitivity to moisture and oxygen often requires more expensive hermetic encapsulation to ensure 25-year reliability. Use of regulated, toxic elements (*e.g.*, Cd) and reliance on rare elements (*e.g.*, Te, In) may limit the potential for large-scale deployment. Current innovation opportunities in thin films include improving module efficiency, improving reliability by introducing more robust materials and cell architectures, and decreasing reliance on rare elements by developing new materials with similar ease of processing.

3˙3. *Emerging thin-film PV.* – In recent years, several new thin-film PV technologies have emerged as a result of intense R&D efforts in materials discovery and device engineering. Key emerging thin-film PV technologies include the following:

– *Copper zinc tin sulfide (Cu_2ZnSnS_4, or CZTS)* is an Earth-abundant alternative to CIGS, with similar processing strategies and challenges [33, 34]. One key challenge involves managing a class of defects known as cation disorder: Uncontrolled interstitution of Cu and Zn cations creates point defects that can hinder charge extraction and reduce the open-circuit voltage [35]. Record certified cell efficiencies have reached 12.6% [18, 36].

– *Dye-sensitized solar cells (DSCs)* are among the most mature of nanomaterial-based PV technologies [37-39]. These photoelectrochemical cells consist of a transparent inorganic scaffold anode (typically nano-porous TiO_2) sensitized with light-absorbing dye molecules (usually ruthenium (Ru) complexes) [40, 41]. Unlike the other solid-state technologies discussed here, DSCs often use a liquid electrolyte to transport ions to a counter electrode, although efficient solid-state devices have also been demonstrated [38, 42, 43]. DSCs have achieved efficiencies of up to 12.3% [44] (12.3% and 8.8% certified cell and module records, respectively [18, 45] and may benefit from low-cost materials, simple assembly, and colorful and flexible modules. Key challenges involve limited long-term stability under illumination and high temperatures, low absorption in the near-infrared, and low open-circuit voltages caused by interfacial recombination.

– *Perovskite solar cells* evolved from solid-state dye-sensitized cells [46, 47] and have quickly become one of the most promising emerging thin-film PV technologies, with leading certified efficiencies reaching 25.2% [18] in 10 years of development. The term "perovskite" refers to the crystal structure, and the most widely investigated perovskite for solar cells is the hybrid organic-inorganic lead halide $CH_3NH_3Pb(I,Cl,Br)_3$. Due to the importance of this emerging technology we will dedicate a section to perovskite solar cell.

– *Organic photovoltaics (OPV)* use organic small molecules [48, 49] or polymers [50, 51] to absorb light. These materials consist mostly of Earth-abundant elements and can be assembled into thin films by large-area, high-throughput deposition methods [52]. Organic multijunction cells may be much easier to fabricate than conventional III-V MJs because of their high defect tolerance and ease of deposition [53]. The recent development of ESLs based on non-fullerene materials permitted to increase the VOC of the cells and improve the efficiency beyond 17% [18]. Key concerns involve inefficient exciton transport [48, 50, 51], poor long-term stability [54], low large-area deposition yield, and low ultimate efficiency limits [55].

– *Colloidal quantum dot photovoltaics (QDPV)* use solution-processed nanocrystals, also known as quantum dots (QDs), to absorb light [56-58]. The ability to tune the bandgap of colloidal metal chalcogenide nanocrystals (primarily PbS) by changing their size allows efficient harvesting of near-infrared photons, as well as the potential for multijunction cells using a single-material system [59, 60]. QDPV technologies are improving consistently, with a record certified cell efficiency of 16.6% [18], and they offer simple room-temperature fabrication and air-stable operation [61]. Key challenges include incomplete understanding of QD surface chemistry [62-65] and low open-circuit voltages that may be limited fundamentally by mid-gap states or inherent disorder in QD films [66]. These emerging thin-film technologies employ nanostructured materials that can be engineered to achieve desired optical and electronic properties. Reliance on Earth-abundant materials and relatively simple processing methods bodes well for large-scale manufacturing and deployment. While these technologies range in maturity from fundamental materials R&D to early commercialization and have not yet been deployed at scale, they offer potentially unique device level properties such as visible transparency, high weight-

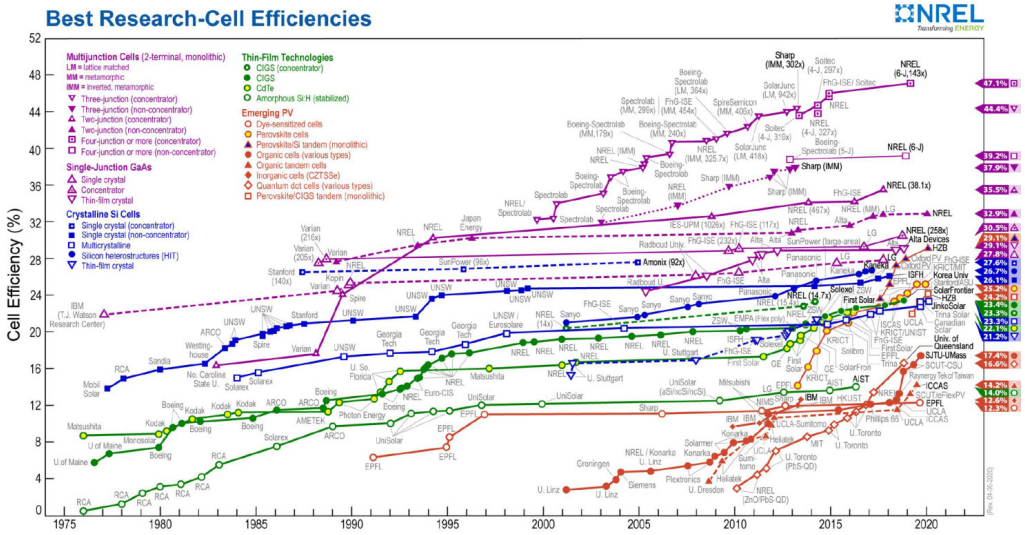

Fig. 10. – Best Research-Cell efficiency reported by the National Renewable Energy Laboratory (NREL, USA) `https://www.nrel.gov/pv/cell-efficiency.html`.

specific power [W/g], and flexible form factors. These qualities could open the door to novel applications for solar PV. In the long-term, emerging thin-film technologies may overcome many of the limitations of today's deployed technologies at low cost, assuming improvements in efficiency and stability are realized.

The developments of all the photovoltaic technologies for 1976 to present are reported by the NREL on the "Best Research-Cell Efficiency Chart" displayed in fig. 10.

4. – Perovskite solar cells

As it happens for many materials, perovskites are named after the Russian mineralogist Lev Aleksevich von Perovski. The discovery was actually made by Gustav Rose in 1839, when he first observed a mineral of calcium titanate ($CaTiO_3$). Thus, the name refers to a crystal structure (fig. 11), rather than a single material, and its corresponding general chemical formula ABX_3. The A site at the centre of the cube (interstitial) is occupied by a monovalent organic or group-I cation, while a divalent metallic cation sits in site B at the corners and oxygen or a halogen occupy position X at the sides of the cube. Alternative views of the crystal lattice see the BX_6 octahedral structures surrounding the interstitial A cation [9]. The relevant perovskite-structured materials for photovoltaic applications are metalorganic lead or tin halides, the basic and most common being methylammonium lead triiodide ($CH_3NH_3PbI_3$) also known as MAPI. IBM researchers had already observed their optoelectronic properties and in 1994 developing a light emitting device [67], however no relevant further activity was registered until 2009, when MAPI was incorporated as a sensitizing dye in a DSC by Myasaka and

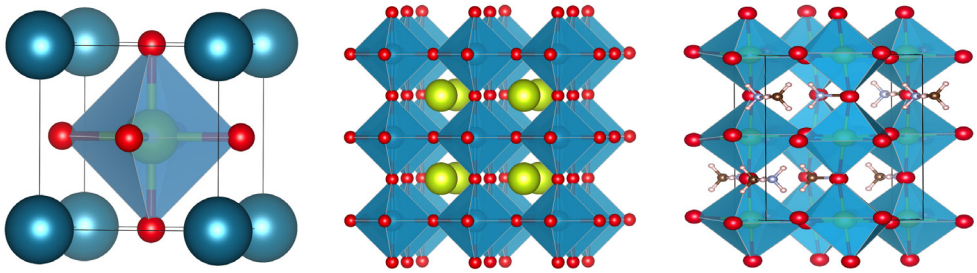

Fig. 11. – Perovskite crystal structure [69]: cubic cell structure (left), crystal overview (middle) and crystal with organic cations (right).

coworkers [68]. The real breakthrough came in 2012, when the group of Prof. Snaith at the University of Oxford developed and published a 10.9% efficient solid state version of DSC in which MAPI perovskite was sandwiched between an alumina layer and the organic semiconductor spiro-OMeTAD [70]. The use of insulating mesoporous Al_2O_3 instead of TiO_2 commonly used as ESL in DSC, clarified that halide perovskite was not a synthesizer for DSCs but a complexly new PV technology. This was just the tip of an iceberg that has now risen so high that perovskites are currently the hot topic in the PV field, with efficiencies that have soared up to 25.2% in less than 10 years (see footnote ([2])). This success has been made thanks to three main properties of halide perovskite, namely i) the exceptional absorbing properties, ii) the good transport properties despite the nanocrystalline structure of the perovskite film and iii) the solution processability of the material.

Optoelectronic properties may be tuned by varying the chemical composition. Specifically, the B-X bond seems to be the one mostly affecting the bandgap of these materials as the conduction and valence bands are composed of p orbitals from B and X ions, respectively [71].

Tuning the gap of the perovskite by halide substitution in $CH_3NH_3Pb(I_{1-x}Br_x)_3$ has attracted interest because of the possibility to continuously range from 1.55 eV ($x = 0$) to 2.2 eV ($x = 1$) varying the I/Br content ratio [72]. The same applies for chlorine substitution for even higher gap structures [73]. One drawback of this solution is the light-induced phase segregation that induces Br-rich phases to form, causing the photo-instability of the photoluminescence and absorption spectrum of the films, something that is not desirable for a solar cell. This is known as Hoke effect and reverses once the films are kept in dark [74]. In a perovskite solar cell this causes a loss in V_{OC} under illumination, because the Br-rich regions are regions where charge carriers recombine, thus causing the voltage loss. The Br concentration at which the phase segregation becomes evident is $x = 0.2$: for this reason, most perovskite chemical compositions have a bromine content below this threshold. A recent study by Mahesh *et al.* has evidenced that another cause of voltage loss is actually the formation of mid-gap trap states arising from imperfections within the perovskite layer and the non-ideal interfaces with the other

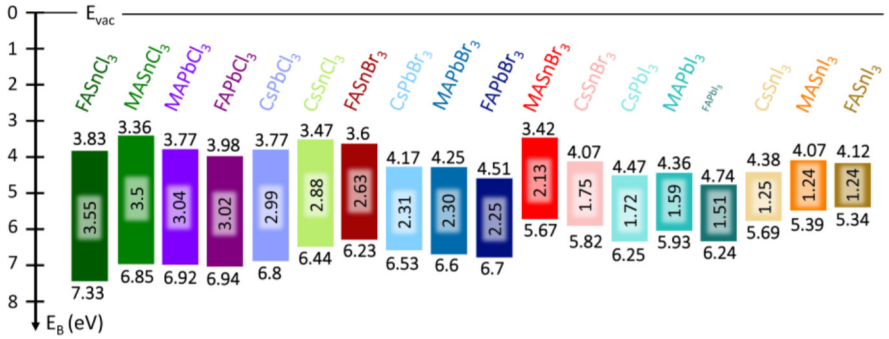

Fig. 12. – Energy levels of different perovskite compositions [86].

layers of the device, causing a loss in radiative efficiency [75]. The X site is not the only one that could undergo substitution. The presence of lead (Pb) is a major concern for health and environmental reasons [76], so its substitution with tin (Sn) or other divalent metals is being looked into [77]. The substitution leads to a 1.1 eV narrow bandgap perovskite. This has proven to be not an easy task as Sn (II) is highly unstable and readily oxidizes to Sn (IV), unsuitable for the perovskite structure [78]. That of stability is the major disadvantage holding perovskites from entering the market, as they should pass IEC standard 61646 to do so [79-81]. In this context, the substitution of the A site has played an important role. The problem of A site cation substitution is finding ions or molecules of the right size that fit and stay in the perovskite structure. In this regard, Goldschmidt tolerance factor comes to aid [82]:

$$t = \frac{(r_A + r_X)}{\sqrt{2}(r_B + r_X)}$$

with r indicating the radius of the ion. If t is in the 0.85 to 1.1 range, then the perovskite structure holds. Formamidinium ($CH(NH_2)_2^+$ - FA^+), cesium (Cs^+) and methylammonium ($CH_3NH_3^+$ - MA^+) satisfy this condition and are widely used [83], however smaller cations from other group-I elements (K^+ and Rb^+) have been used, though they might not stay in the interstitials [84, 85]. The variation in size at the A site causes distortions in the B-X bond and tilting of the octahedral structures (fig. 11 on the right), therefore it also has a slight influence on the bandgap. A summary of the energy levels of some compositions of perovskite solar cells is shown is fig. 12 [86].

Since perovskite is an intrinsic semiconductor, in order to be exploited in PV devices, it must be sandwiched between HSL and PSL forming a p-i-n heterojunction. Depending on which layer is deposited first and on the structure of the cell, we have different architectures, schematized in fig. 13: mesoscopic n-i-p, planar n-i-p and planar p-i-n. These will be described in the following sections.

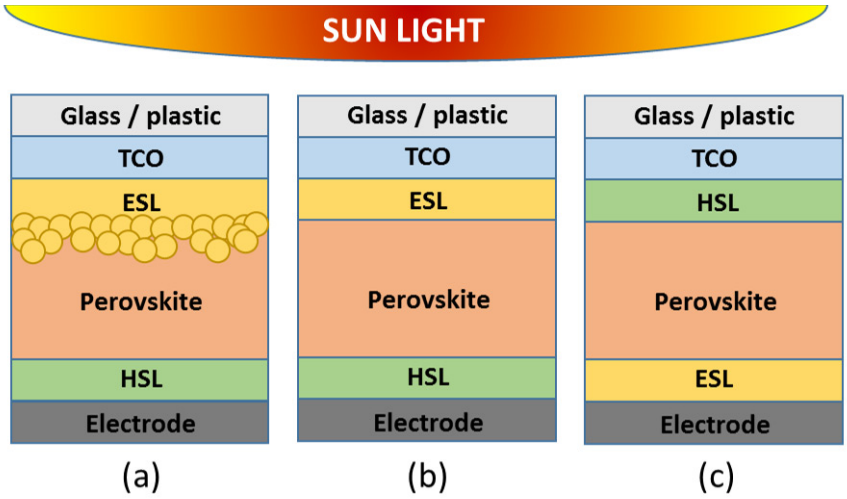

Fig. 13. – Schematics of the different perovskite solar cell architectures (a) mesoscopic n-i-p cell, (b) planar n-i-p cell, (c) p-i-n cell. HSL can be polymers (PTAA, P3HT), molecules (Spiro-OMeTAD) or inorganic materials such as NiO, while ESL can be C60, PCBM, SnO_2, TiO_2 etc. Here TCO is for Transparent Conductive Oxide such as ITO, FTO etc.

4˙1. *Perovskite thin-film crystallization.* – The perovskite layer is at the core of PSCs, whose quality greatly determines the PV performance. So far, many processes have been exploited to prepare perovskite layer, which could be simply divided into two kinds, one-step and two-step methods. The one-step method has been adopted in pioneering works [47, 87]. However, the naturally crystallized perovskite often exhibited an anisotropic growth, leading to low uniformity and poor coverage [88, 89]. This phenomenon limited the PV performance in the early attempts and has been solved by the anti-solvent strategy [90-92]. Here a drop of solvent, in which the perovskite is insoluble, is casted on the top of deposited perovskite precursor permitting the precipitation of the perovskite crystal. Such solvent quenching technique has been also extended to vacuum quenching and gas quenching. For the two-step method (see fig. 14), PbI_2 layer is first deposited, followed by the conversion to perovskite in MAI solution [93-95]. Since the deposition processes and the control strategy of the PbI_2 layer are versatile and flexible, uniform and full coverage PbI_2 layer could be easily obtained, which tends to improve the quality of the perovskite layer. The first successful work on the two-step method for PSCs was reported by Burschka *et al.* in 2013, which obtained a PCE of 15% [95]. The progresses made on the understanding of the reaction/growth mechanism of the two-step method resulted in the optimization of the processes, which well improved the perovskite quality and enhanced the device performance. By combining the second spin-coating step with the optimization on MAI concentration, the perovskite grain size was optimized to absorb most of visible light with the minimum recombination loss, which promoted the PCE to over 16%. A novel interdiffusion strategy based on the two spin-coating

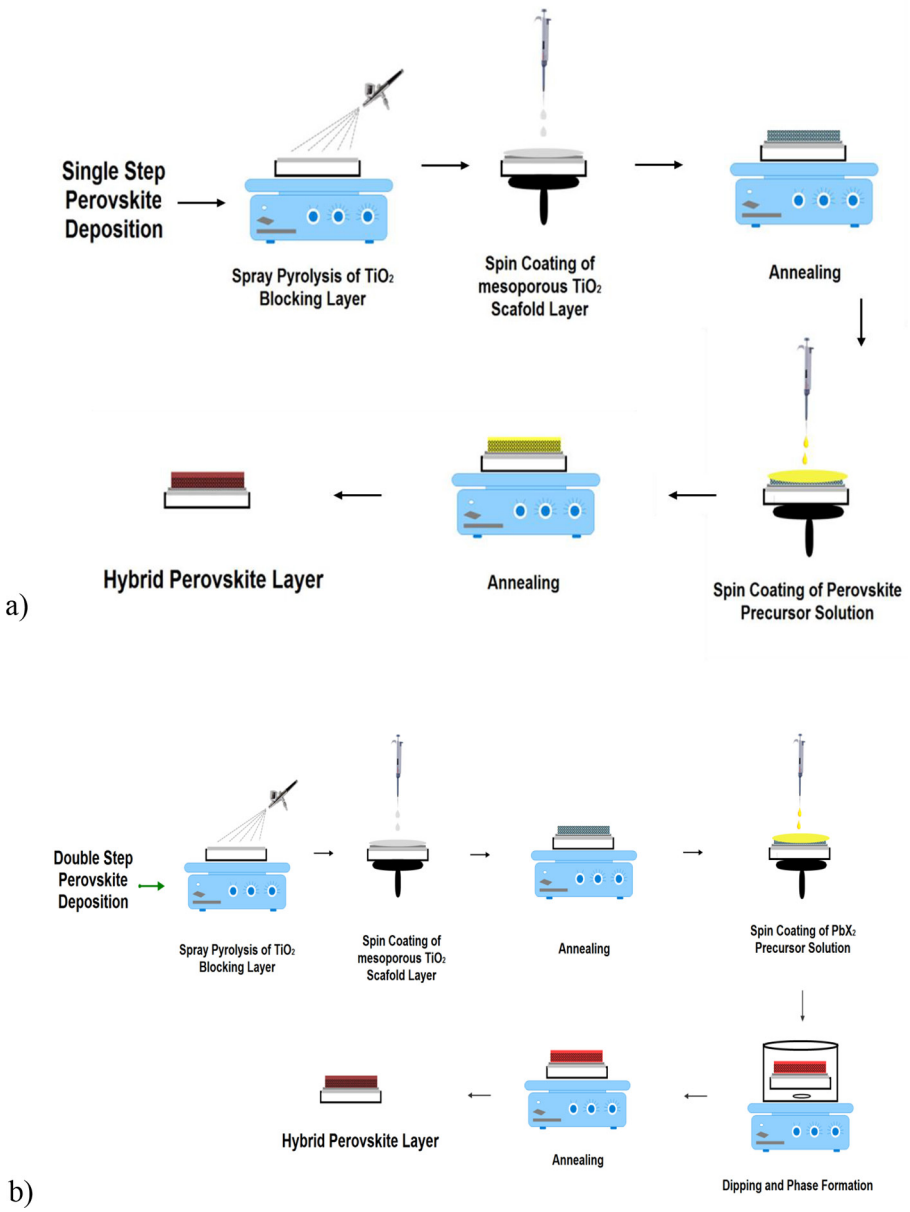

Fig. 14. – Single step (a) *vs.* double step (b) perovskite layer deposition.

step process further improved the perovskite quality and promoted the PCE to about 19% [96]. Recently, by applying a new Pb-I precursor of PbI_2(DMSO), high-quality $FAPbI_3$/$MAPbBr_3$ perovskite was obtained through intramolecular exchange between FA/MA with DMSO, which boosted the PCE to over 20% [97]. Therefore, the two-step method has been well proved to be an effective approach to synthesize high-quality thin perovskite for high-performance PSCs even out of the glove-box.

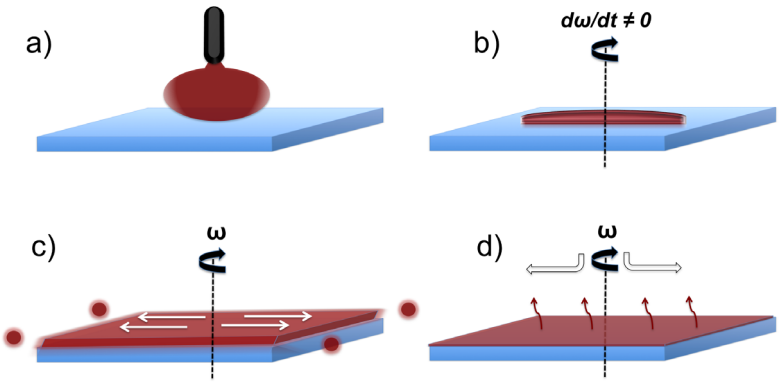

Fig. 15. – Four steps of spin coating as (a) deposition, (b) spin-up, (c) spin-off and (d) evaporation.

4˙2. *Deposition techniques of perovskite thin film.* – In this section we will present the different techniques developed so far to deposit the halide perovskite absorber. Some of them are common to other emerging thin-film photovoltaics and the description provided here could be adapted to also these other cases. We can divide all these technique in coating processes from liquid phase and physical deposition such as thermal evaporation.

4˙2.1. Spin coating. Spin coating is inherently a batch process the outcome of which is a solidified thin coating on a rigid flat disk, plate, or slightly curved bowl or lens. The process can be divided into four stages: deposition, spin-up, spin-off, and evaporation (see fig. 15). The second may overlap the first but the first three stages are sequential [98].

The spin-coating method was the first method used for the precursor deposition for PSCs by Burschka *et al.*, which afforded the PSCs with a PCE of 15% [93]. Most of the following works adopted this method due to its simplicity, low cost, and efficient [96, 97, 99]. The highest reported PCE of 25% was also achieved by spin coating method [18]. However, the main disadvantage of this method is that it is only suitable for small device fabrication, which would surely limit the commercialization of PSCs.

4˙2.2. Blade coating. The blade coating method (fig. 16) is a large-area scalable method, which is very famous for preparing TiO_2 mesoporous film in dye-sensitized solar cells (in fig. 15(a)). However, very few successful cases have been reported for fabricating PbI_2 layer by the blade coating method because the over grown crystals and pinholes due to the natural dry of PbI_2 solution could not be well solved. Inspired by the rapid evaporation of solvent in the spin-coating method, Razza *et al.* employed an air-flow–assisted PbI_2 doctor-blade deposition, in which DMF solvent was rapidly driven away by air flow during the deposition process [100]. Later Yaghoobi Nia *et al.* reported a perovskite solar Module using blade coating deposition fully in the ambient condition reaching 17.7% on 1 cm^2 and 11.5% on 50 cm^2 active area [101]. Recently, Zhang showed the efficiency of 13.32% on 53.6 cm^2 active area using a sequential two-step blade coating of Perovksite layer as shown in fig. 15(b) [102].

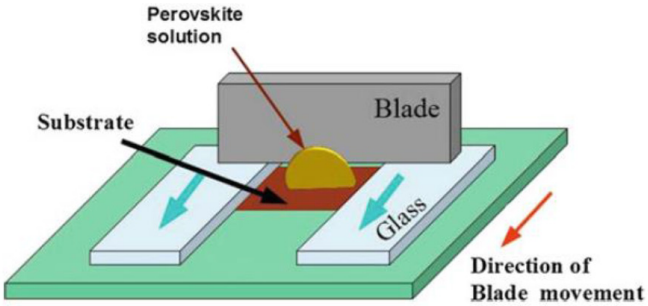

a)

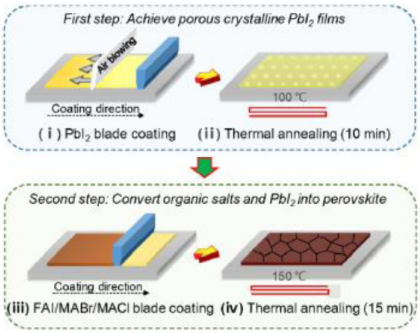

b)

Fig. 16. – (a) Blade coating system [103]. (b) Schematic illustration of the sequential two-step blade coating of perovskite films: (i) blade-coating of PbI2 films assisted with gas blowing, (ii) Thermal annealing of PbI2 films, (iii) blade-coating of FAI/MABr/MACl, and (iv) thermal annealing of the perovskite film [102].

4˙2.3. Slot-die coating. For commercialization purpose, developing mature and scalable manufacturing technologies is necessary and slot-die coating permits to reach this goal also on flexible surfaces (roll-to-roll coating). Several groups have made attempts to achieve this by employing manufacturing technologies to deposit precursors. For example, Hwang *et al.* employed the scalable printing method of sequential slot-die coating to deposit PbI_2 precursors [104], accompanied with the gas-quenching process to evaporate the solvent quickly, mimicking the "quenching" step in spin-coating method, as shown in fig. 17. This approach obtained a uniform pinhole-free PbI_2 precursor layer, comparable to that prepared by the spin-coating method. The slot-die coating method was also successfully developed to prepare ZnO and P3HT layers, which made the whole procedure compatible to the famous roll-to-roll manufacturing technology. The best PCE of 14.7% was achieved by the PSCs fabricated by all slot-die coating processes under ambient conditions [84].

4˙2.4. Vapor deposition. Vapor deposition is characterized by a process in which the material goes from a condensed phase to a vapor phase and then back to a thin-film con-

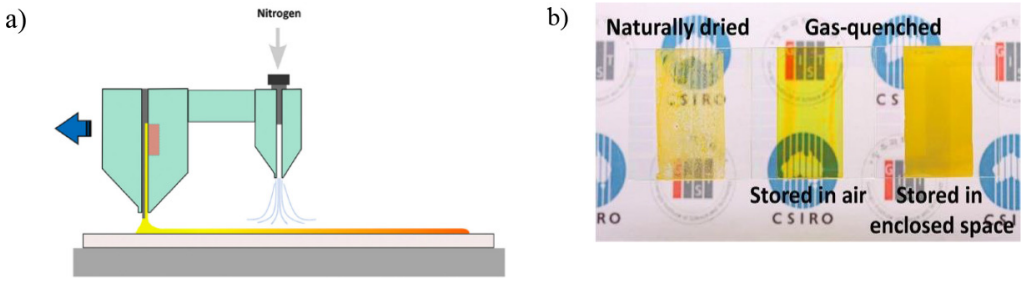

Fig. 17. – (a) Schematic illustration of slot-die coating with a gas-quenching process for the fabrication of pinhole-free PbI2 layer. (b) Photographs of slot-die coated PbI2 films under various coating conditions. The figures are selected from ref. [104].

densed phase. The vapor deposition method (fig. 18) has also found its success in PSCs fabrication, which was first reported by Liu *et al.* [105]. In their work, $MAPbI_{3-x}Cl_x$ was deposited by a dual-source vapor deposition, which achieved a PCE of 15%. Then, several successful works on depositing precursors by vapor method were reported. For example, Chen *et al.* have deposited the $PbCl_2$ precursor by vapor deposition at a high vacuum chamber (base pressure < 1 Å $\sim 10^{-6}$ Torr) [106]. This $PbCl_2$ precursor was then subjected to MAI vapor for conversion to $MAPbI_{3-x}Cl_x$ with large-scale homogeneous structure. When used in PSCs, a PCE as high as 15.4% was obtained, which highlighted the vapor method as a promising technology for potential commercial production. Jia Li *et al.* showed an efficacy of 18% using the thermally Co-evaporated method for deposition of perovskite layer [107].

4˙2.5. Atomic Layer Deposition (ALD). An atomic layer deposition (ALD) method is reported by Sutherland *et al.* to prepare PbI_2 precursor [109]. As a low-vacuum and low-temperature deposition technique, ALD could produce uniform and conformal films over large areas with the thickness controlled at atomic precision. The whole ALD-based procedure began with the growth of the PbS seed layer by ALD from controlled alternating pulses of H_2S and $Pb(tmhd)_2$ precursors. Then, the PbS layer was converted to PbI_2 through exposure to iodine gas generated from solid iodine in a closed system, followed by the conversion to $MAPbI_3$ in MAI solution. Since the ALD method was not limited by substrate shape, the deposition of the conformal $MAPbI_3$ layer on the spherical shape substrate was also obtained, which enabled lasing on spherical resonators [110]. However, the growth rate of the ALD method is very slow (100 nm needed several hours), which is not suitable for large-scale manufacturing. Furthermore, the post conversion of ALD layers (PbS and PbI_2) should be difficult due to their high compactness, especially for large film thickness.

4˙3. *Large area.* – Development in perovskite solar cells permitted also to go beyond the small are laboratory cells and many efforts have been made worldwide to scale the technology to the module level. The results of the CHOSE laboratory in this field are shown in fig. 19.

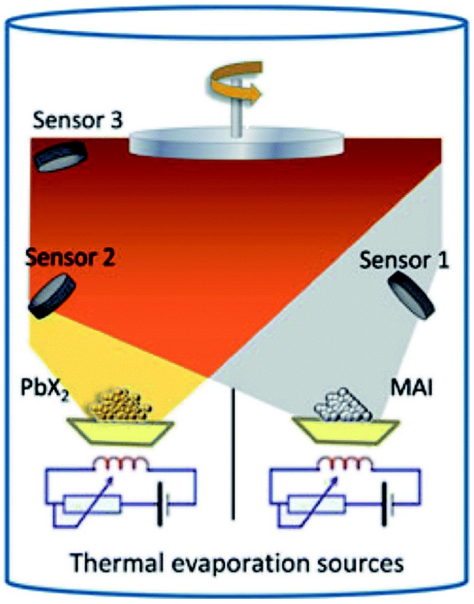

Fig. 18. – Illustration of the dual-source vacuum deposition instrument. The PbX2 (X = I, Cl) and CH3NH3I (MAI) precursors are thermally evaporated in vacuum. The deposition rate and thickness are monitored using quartz microbalances. The figure is taken from ref. [108].

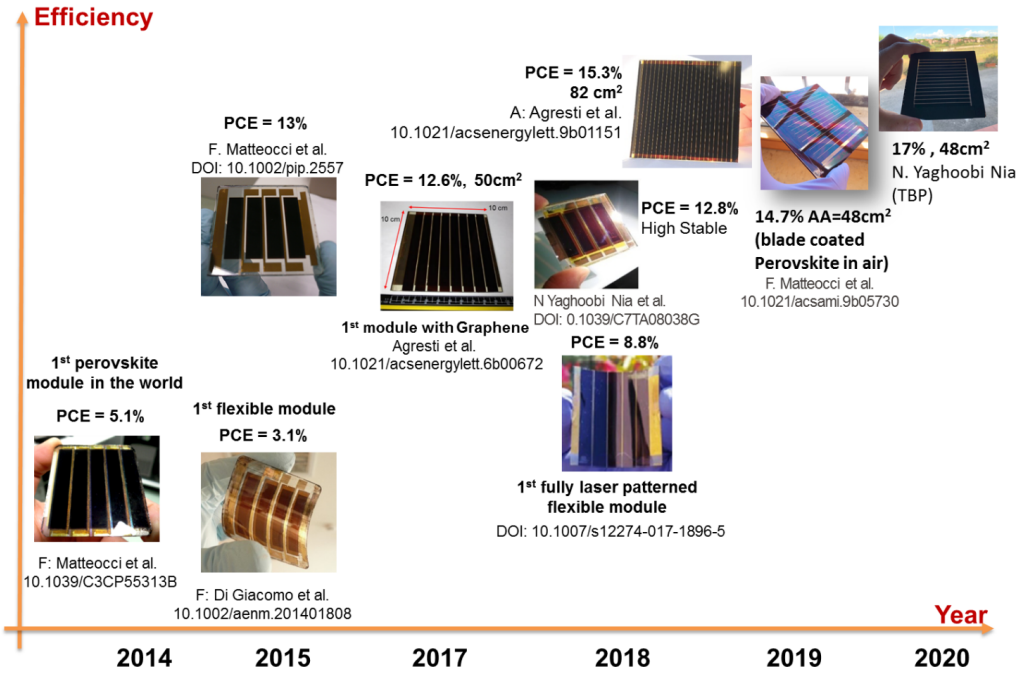

Fig. 19. – Perovskite module development at the Centre for Hybrid and Organic solar Energy (CHOSE), University of Rome Tor Vergata.

We should also point out that PSCs are also suitable as top cell in perovskite/silicon tandem and efficiencies beyond 29% have been already demonstrated (see fig. 10).

5. – Conclusions

Electricity generation from renewable sources is crucial for the urgent request of decarbonisation of the world's energy system. This has driven the development of photovoltaics till the point that PV electricity is becoming the economic choice for utilities providers. In this short overview, we have mainly focused on photovoltaics showing how reach is the technology portfolio that can be used to convert solar energy into electricity. The possibility to adapt PV to the application requests by varying aspect (opaque, semitransparent, coloured), structural properties (rigid, semi-rigid, conformable, flexible) physical properties (normal illumination conditions, low light, concentrated light) or production processes (semiconductor process, printing process) will permit a pervasive use of PV in different field from the traditional utility scale energy production to BIPV and energy harvesters for Internet of Things. At the same time, advanced PV concepts should still be exploited at industry scale or even demonstrated at laboratory level. Here we could mention some concepts as halide perovskite, silicon tandem, hot-carrier, carrier multiplications, Bose condensation in cavities as well as the integration between PV and other energy generation system such as thermoelectrics. In few words, differently from many other energy production systems, PV is moving in the field of Information and Communication technologies which has a faster innovation and development time with respect to typical industrial engineering. Thus, the future of PV is still open for strong innovations with the aim to reach the upper theoretical limit of its efficiency that is close to the Carnot limit of 95%, well above the present record of 47.1% (see fig. 10).

REFERENCES

[1] Metz A. *et al.*, *International Technology Roadmap for Photovoltaics (ITRPV) 2017* (ITRPV, VDMA) 2017, pp. 1–40.
[2] Green M. A., Dunlop E. D., Hohl-Ebinger J., Yoshita M., Kopidakis N. and Ho-Baillie A. W. Y., *Prog. Photovolt. Res. Appl.*, **28** (2020) 3.
[3] Shaheen S. E., Brabec C. J., Sariciftci N. S., Padinger F., Fromherz T. and Hummelen J. C., *Appl. Phys. Lett.*, **78** (2001) 841.
[4] Halls J. J. M., Pichler K., Friend R. H., Moratti S. C. and Holmes A. B., *Appl. Phys. Lett.*, **68** (1996) 3120.
[5] Brabec C. J. and Durrant J. R., *MRS Bull.*, **33** (2011) 670.
[6] Battaglia C., Cuevas A. and De Wolf S., *Energy Environ. Sci.*, **9** (2016) 1552.
[7] Tanaka M., Taguchi M., Matsuyama T., Sawada T., Tsuda S., Nakano S., Hanafusa H. and Kumano Y., *Jpn. J. Appl. Phys.*, **31** (1992) 3518.
[8] Martini M. T. L., Serenelli L., Menchini F., Izzi M., Asquini R., de Cesare G. and Caputo D., *EU PVSEC 2017 – 33nd European Photovoltaic Solar Energy Conference Exhibition, Conf. Proc.*, **1** (2017) pp. 773–776.
[9] Johnsson M. and Lemmens P., *Handb. Magn. Adv. Magn. Mater.*, **4** (2007) 1, https://doi.org/10.1002/9780470022184.hmm411.

[10] Meng L., Zhang Y., Wan X., Li C., Zhang X., Wang Y., Ke X., Xiao Z., Ding L., Xia R., Yip H. L., Cao Y. and Chen Y., *Science*, **361** (2018) 1094.
[11] O'Regan B. and Grätzel M., *Nature*, **353** (1991) 737.
[12] Polman A., Knight M., Garnett E. C., Ehrler B. and Sinke W. C., *Science*, **352** (2016) 4424.
[13] Hagfeldt A., in *Ambio*, Vol. **41** (Springer) 2012, pp. 151–155.
[14] Hayes M., Martel B., Alam G. W., Lignier H., Dubois S., Pihan E. and Palais O., *Phys. Status Solidi*, **216** (2019) 1900321.
[15] Jean J., Brown P. R., Jaffe R. L., Buonassisi T. and Bulović V., *Energy Environ. Sci.*, **8** (2015) 1200.
[16] Wertz R. *et al.*, *International Technology Roadmap for Fotovoltaics (ITRPV), 2014 Results*, 6th edition, April 2015, pp. 1–38.
[17] Czochralski J., *Z. Phys. Chem.*, **92U** (2017) 219.
[18] Best Research-Cell Efficiency Chart | Photovoltaic Research | NREL, `https://www.nrel.gov/pv/cell-efficiency.html` (accessed 13 July 2020).
[19] Yablonovitch E., Gmitter T., Harbison J. P. and Bhat R., *Appl. Phys. Lett.*, **51** (1987) 2222.
[20] Jones-Albertus R., Becker E., Bergner R., Bilir T., Derkacs D., Fidaner O., Jory D., Liu T., Lucow E., Misra P., Pickett E., Suarez F., Sukiasyan A., Sun T., Zhang L., Sabnis V., Wiemer M. and Yuen H., in *Materials Research Society Symposium Proceedings*, Vol. **1538** (Cambridge University Press) 2013, pp. 161–166.
[21] King R. R., Bhusari D., Larrabee D., Liu X. Q., Rehder E., Edmondson K., Cotal H., Jones R. K., Ermer J. H., Fetzer C. M., Law D. C. and Karam N. H., in *Progress in Photovoltaics: Research and Applications*, Vol. **20** (John Wiley and Sons Ltd) 2012, pp. 801–815.
[22] Chiu P. T., Law D. C., Woo R. L., Singer S. B., Bhusari D., Hong W. D., Zakaria A., Boisvert J., Mesropian S., King R. R. and Karam N. H., *IEEE J. Photovolt.*, **4** (2014) 493.
[23] *International Technology Roadmap for Photovoltaic (ITRPV)*, `https://itrpv.vdma.org/`.
[24] Luque Antonio and Hegedus Steven (Editors), *Handbook of Photovoltaic Science and Engineering* (Wiley) 2003, ISBN:9780471491965; DOI:10.1002/0470014008.
[25] Staebler D. L. and Wronski C. R., *Appl. Phys. Lett.*, **31** (1977) 292.
[26] *CdTe PV: Real and Perceived EHS Risks (Conference)*, `https://www.osti.gov/biblio/15004247` (accessed 13 July 2020).
[27] Kessler F. and Rudmann D., *Sol. Energy*, **77** (2004) 685.
[28] Hetzer M. J., Strzhemechny Y. M., Gao M., Contreras M. A., Zunger A. and Brillson L. J., *Appl. Phys. Lett.*, **86** (2005) 162105.
[29] Werner J. H., Mattheis J. and Rau U., in *Thin Solid Films*, Vols. **480–481** (Elsevier) 2005, pp. 399–409.
[30] Nishiwaki S., Siebentritt S., Walk P. and Lux-Steiner M. C., *Prog. Photovolt. Res. Appl.*, **11** (2003) 243.
[31] Hsu D. D., O'Donoughue P., Fthenakis V., Heath G. A., Kim H. C., Sawyer P., Choi J. K. and Turney D. E., *J. Ind. Ecol.*, **16** (2012) S122.
[32] Kim H. C., Fthenakis V., Choi J.-K. and Turney D. E., *J. Ind. Ecol.*, **16** (2012) S110.
[33] Todorov T. K., Tang J., Bag S., Gunawan O., Gokmen T., Zhu Y. and Mitzi D. B., *Adv. Energy Mater.*, **3** (2013) 34.
[34] Katagiri H., Jimbo K., Maw W. S., Oishi K., Yamazaki M., Araki H. and Takeuchi A., *Thin Solid Films*, **517** (2009) 2455.

[35] Hobson T. D. C., Phillips L. J., Hutter O. S., Durose K. and Major J. D., *Appl. Phys. Lett.*, **116** (2020) 261101.
[36] Wang W., Winkler M. T., Gunawan O., Gokmen T., Todorov T. K., Zhu Y. and Mitzi D. B., *Adv. Energy Mater.*, **4** (2014) 1301465.
[37] Hagfeldt A., Boschloo G., Sun L., Kloo L. and Pettersson H., *Chem. Rev.*, **110** (2010) 6595.
[38] Grätzel M., *Inorg. Chem.*, **44** (2005) 6841.
[39] Grätzel M., *J. Photochem. Photobiol. C Photochem. Rev.*, **4** (2003) 145.
[40] Nazeeruddin M. K., Péchy P., Renouard T., Zakeeruddin S. M., Humphry-Baker R., Cointe P., Liska P., Cevey L., Costa E., Shklover V., Spiccia L., Deacon G. B., Bignozzi C. A. and Grätzel M., *J. Am. Chem. Soc.*, **123** (2001) 1613.
[41] Snaith H. J. and Schmidt-Mende L., *Adv. Mater.*, **19** (2007) 3187.
[42] Chung I., Lee B., He J., Chang R. P. H. and Kanatzidis M. G., *Nature*, **485** (2012) 486.
[43] Bach U., Lupo D., Comte P., Moser J. E., Weissörtel F., Salbeck J., Spreitzer H. and Grätzel M., *Nature*, **395** (1998) 583.
[44] Yella A., Lee H. W., Tsao H. N., Yi C., Chandiran A. K., Nazeeruddin M. K., Diau E. W. G., Yeh C. Y., Zakeeruddin S. M. and Grätzel M., *Science*, **334** (2011) 629.
[45] Green M. A., *Prog. Photovolt. Res. Appl.*, **23** (2015) 1202.
[46] Kim H. S., Lee C. R., Im J. H., Lee K. B., Moehl T., Marchioro A., Moon S. J., Humphry-Baker R., Yum J. H., Moser J. E., Grätzel M. and Park N. G., *Sci. Rep.*, **2** (2012) 591.
[47] Lee M. M., Teuscher J., Miyasaka T., Murakami T. N. and Snaith H. J., *Science*, **338** (2012) 643.
[48] Peumans P., Yakimov A. and Forrest S. R., *J. Appl. Phys.*, **93** (2003) 3693.
[49] Riede M. *et al.*, *Nanotechnology*, **19** (2008) 424001.
[50] Günes S., Neugebauer H. and Sariciftci N. S., *Chem. Rev.*, **107** (2007) 1324.
[51] Li G., Zhu R. and Yang Y., *Nat. Photon.*, **6** (2012) 153.
[52] Krebs F. C., *Sol. Energy Mater. Sol. Cells*, **93** (2009) 394.
[53] Kim J. Y., Lee K., Coates N. E., Moses D., Nguyen T. Q., Dante M. and Heeger A. J., *Science*, **317** (2007) 222.
[54] Kawano K., Pacios R., Poplavskyy D., Nelson J., Bradley D. D. C. and Durrant J. R., *Sol. Energy Mater. Sol. Cells*, **90** (2006) 3520.
[55] Lunt R. R., Osedach T. P., Brown P. R., Rowehl J. A. and Bulović V., *Adv. Mater.*, **23** (2011) 5712.
[56] Lan X., Masala S. and Sargent E. H., *Nat. Mater.*, **13** (2014) 233.
[57] Semonin O. E., Luther J. M. and Beard M. C., *Mater. Today*, **15** (2012) 508.
[58] Tang J. and Sargent E. H., *Adv. Mater.*, **23** (2011) 12.
[59] Choi J. J., Wenger W. N., Hoffman R. S., Lim Y. F., Luria J., Jasieniak J., Marohn J. A. and Hanrath T., *Adv. Mater.*, **23** (2011) 3144.
[60] Wang X., Koleilat G. I., Tang J., Liu H., Kramer I. J., Debnath R., Brzozowski L., Barkhouse D. A. R., Levina L., Hoogland S. and Sargent E. H., *Nat. Photon.*, **5** (2011) 480.
[61] Chuang C. H. M., Brown P. R., Bulović V. and Bawendi M. G., *Nat. Mater.*, **13** (2014) 796.
[62] Brown P. R., Kim D., Lunt R. R., Zhao N., Bawendi M. G., Grossman J. C. and Bulović V., *ACS Nano*, **8** (2014) 5863.

[63] Ip A. H., Thon S. M., Hoogland S., Voznyy O., Zhitomirsky D., Debnath R., Levina L., Rollny L. R., Carey G. H., Fischer A., Kemp K. W., Kramer I. J., Ning Z., Labelle A. J., Chou K. W., Amassian A. and Sargent E. H., *Nat. Nanotechnol.*, **7** (2012) 577.
[64] Jasieniak J., Califano M. and Watkins S. E., in *ACS Nano*, Vol. **5** (American Chemical Society) 2011, pp. 5888–5902.
[65] Tang J., Kemp K. W., Hoogland S., Jeong K. S., Liu H., Levina L., Furukawa M., Wang X., Debnath R., Cha D., Chou K. W., Fischer A., Amassian A., Asbury J. B. and Sargent E. H., *Nat. Mater.*, **10** (2011) 765.
[66] Zhitomirsky D., Voznyy O., Levina L., Hoogland S., Kemp K. W., Ip A. H., Thon S. M. and Sargent E. H., *Nat. Commun.*, **5** (2014) 3803.
[67] Mitzi D. B., Feild C. A., Harrison W. T. A. and Guloy A. M., *Nature*, **369** (1994) 467.
[68] Kojima A., Teshima K., Shirai Y. and Miyasaka T., *J. Am. Chem. Soc.*, **131** (2009) 6050.
[69] Chen Q., De Marco N., Yang Y., Bin Song T., Chen C. C., Zhao H., Hong Z., Zhou H. and Yang Y., *Nano Today*, **10** (2015) 355.
[70] Lee M. M., Teuscher J., Miyasaka T., Murakami T. N. and Snaith H. J., *Science*, **338** (2012) 643.
[71] Frost J. M., Butler K. T., Brivio F., Hendon C. H., Van Schilfgaarde M. and Walsh A., *Nano Lett.*, **14** (2014) 2584.
[72] Atourki L., Vega E., Marí B., Mollar M., Ait Ahsaine H., Bouabid K. and Ihlal A., *Appl. Surf. Sci.*, **371** (2016) 112.
[73] Comin R., Walters G., Thibau E. S., Voznyy O., Lu Z. H. and Sargent E. H., *J. Mater. Chem. C*, **3** (2015) 8839.
[74] Hoke E. T., Slotcavage D. J., Dohner E. R., Bowring A. R., Karunadasa H. I. and McGehee M. D., *Chem. Sci.*, **6** (2015) 613.
[75] Mahesh S., Ball J. M., Oliver R. D. J., McMeekin D. P., Nayak P. K., Johnston M. B. and Snaith H. J., *Energy Environ. Sci.*, **13** (2020) 258.
[76] Li J., Cao H. L., Bin Jiao W., Wang Q., Wei M., Cantone I., Lü J. and Abate A., *Nat. Commun.*, **11** (2020) 310.
[77] Ke W. and Kanatzidis M. G., *Nat. Commun.*, **10** (2019) 965.
[78] Lee S. J., Shin S. S., Kim Y. C., Kim D., Ahn T. K., Noh J. H., Seo J. and Il Seok S., *J. Am. Chem. Soc.*, **138** (2016) 3974.
[79] Leijtens T., Eperon G. E., Noel N. K., Habisreutinger S. N., Petrozza A. and Snaith H. J., *Adv. Energy Mater.*, **5** (2015) 1500963.
[80] Holzhey P., Yadav P., Turren-Cruz S. H., Grätzel M., Hagfeldt A. and Saliba M., *Mater. Today*, **29** (2019) 10, DOI:10.1016/j.mattod.2018.10.017.
[81] Asghar M. I., Zhang J., Wang H. and Lund P. D., *Renew. Sustain. Energy Rev.*, **77** (2017) 131.
[82] Goldschmidt V. M., *Ber. Dtsch. Chem. Gesellschaft A B Ser.*, **60** (1927) 1263.
[83] Saliba M., Matsui T., Seo J. Y., Domanski K., Correa-Baena J. P., Nazeeruddin M. K., Zakeeruddin S. M., Tress W., Abate A., Hagfeldt A. and Grätzel M., *Energy Environ. Sci.*, **9** (2016) 1989.
[84] Bu T., Liu X., Zhou Y., Yi J., Huang X., Luo L., Xiao J., Ku Z., Peng Y., Huang F., Cheng Y. B. and Zhong J., *Energy Environ. Sci.*, **10** (2017) 2509.
[85] Saliba M., Matsui T., Domanski K., Seo J. Y., Ummadisingu A., Zakeeruddin S. M., Correa-Baena J. P., Tress W. R., Abate A., Hagfeldt A. and Grätzel M., *Science*, **354** (2016) 206.

[86] Tao S., Schmidt I., Brocks G., Jiang J., Tranca I., Meerholz K. and Olthof S., *Nat. Commun.*, **10** (2019) 2560, DOI:10.1038/s41467-019-10468-7.
[87] D'Innocenzo V., Grancini G., Alcocer M. J. P., Kandada A. R. S., Stranks S. D., Lee M. M., Lanzani G., Snaith H. J. and Petrozza A., *Nat. Commun.*, **5** (2014) 3586.
[88] Dualeh A., Tétreault N., Moehl T., Gao P., Nazeeruddin M. K. and Grätzel M., *Adv. Funct. Mater.*, **24** (2014) 3250.
[89] Yantara N., Sabba D., Yanan F., Kadro J. M., Moehl T., Boix P. P., Mhaisalkar S., Grätzel M. and Grätzel C., *Chem. Commun.*, **51** (2015) 4603.
[90] Jeon N. J., Noh J. H., Kim Y. C., Yang W. S., Ryu S. and Il Seok S., *Nat. Mater.*, **13** (2014) 897.
[91] Bi D., Yi C., Luo J., Décoppet J. D., Zhang F., Zakeeruddin S. M., Li X., Hagfeldt A. and Grätzel M., *Nat. Energy*, **1** (2016) 16142.
[92] Xiao M., Huang F., Huang W., Dkhissi Y., Zhu Y., Etheridge J., Gray-Weale A., Bach U., Cheng Y. B. and Spiccia L., *Angew. Chem. Int. Ed.*, **53** (2014) 9898.
[93] Burschka J., Pellet N., Moon S. J., Humphry-Baker R., Gao P., Nazeeruddin M. K. and Grätzel M., *Nature*, **499** (2013) 316.
[94] Liang K., Mitzi D. B. and Prikas M. T., *Chem. Mater.*, **10** (1998) 403.
[95] Zhao J. J., Wang P., Liu Z. H., Wei L. Y., Yang Z., Chen H. R., Fang X. Q., Liu X. L. and Mai Y. H., *Dalt. Trans.*, **44** (2015) 17841.
[96] Dong Q., Yuan Y., Shao Y., Fang Y., Wang Q. and Huang J., *Energy Environ. Sci.*, **8** (2015) 2464.
[97] Yang W. S., Noh J. H., Jeon N. J., Kim Y. C., Ryu S., Seo J. and Il Seok S., *Science*, **348** (2015) 1234.
[98] Scriven L. E., *MRS Proc.*, **121** (1988) 717, DOI:10.1557/proc-121-717.
[99] Yaghoobi Nia N., Lamanna E., Zendehdel M., Palma A. L., Zurlo F., Castriotta L. A. and Di Carlo A., *Small*, **15** (2019) 1904399.
[100] Razza S., Di Giacomo F., Matteocci F., Cinà L., Palma A. L., Casaluci S., Cameron P., D'Epifanio A., Licoccia S., Reale A., Brown T. M. and Di Carlo A., *J. Power Sources*, **277** (2015) 286.
[101] Yaghoobi Nia N., Giordano F., Zendehdel M., Cinà L., Palma A. L., Medaglia P. G., Zakeeruddin S. M., Grätzel M. and Di Carlo A., *Nano Energy*, **69** (2020) 104441.
[102] Zhang J., Bu T., Li J., Li H., Mo Y., Wu Z., Liu Y., Zhang X. L., Cheng Y. B. and Huang F., *J. Mater. Chem. A*, **8** (2020) 8447.
[103] Deng Y., Peng E., Shao Y., Xiao Z., Dong Q. and Huang J., *Energy Environ. Sci.*, **8** (2015) 1544.
[104] Hwang K., Jung Y. S., Heo Y. J., Scholes F. H., Watkins S. E., Subbiah J., Jones D. J., Kim D. Y. and Vak D., *Adv. Mater.*, **27** (2015) 1241.
[105] Liu M., Johnston M. B. and Snaith H. J., *Nature*, **501** (2013) 395.
[106] Chen C.-W., Kang H.-W., Hsiao S.-Y., Yang P.-F., Chiang K.-M. and Lin H.-W., *Adv. Mater.*, **26** (2014) 6647.
[107] Li J., Wang H., Chin X. Y., Dewi H. A., Vergeer K., Goh T. W., Lim J. W. M., Lew J. H., Loh K. P., Soci C., Sum T. C., Bolink H. J., Mathews N., Mhaisalkar S. and Bruno A., *Joule*, **4** (2020) 1035, DOI:10.1016/j.joule.2020.03.005.
[108] Ono L. K., Leyden M. R., Wang S. and Qi Y., *J. Mater. Chem. A*, **4** (2016) 6693.
[109] Sutherland B. R., Hoogland S., Adachi M. M., Wong C. T. O. and Sargent E. H., *ACS Nano*, **8** (2014) 10947.
[110] Yi C., Luo J., Meloni S., Boziki A., Ashari-Astani N., Grätzel C., Zakeeruddin S. M., Röthlisberger U. and Grätzel M., *Energy Environ. Sci.*, **9** (2016) 656.